Pharm Res (2019) 36: 68
https://doi.org/10.1007/s11095-019-2598-3

RESEARCH PAPER

Polyelectrolyte Carboxymethyl Cellulose for Enhanced Delivery of Doxorubicin in MCF7 Breast Cancer Cells: Toxicological Evaluations in Mice Model

Vahid Shafiei-Irannejad[1,2] • Mahdi Rahimi[3,4,5] • Mojtaba Zarei[6] • Roshan Dinparast-isaleh[1] • Saman Bahrambeigi[1] • Alireza Alihemmati[3] • Salman Shojaei[5] • Zarrin Ghasemi[5] • Bahman Yousefi[6]

Received: 16 January 2019 / Accepted: 26 February 2019 / Published online: 18 March 2019

ABSTRACT

Purpose Chemotherapy as an important tool for cancer treatment faces many obstacles such as multidrug resistance and adverse toxic effects on healthy tissues. Drug delivery systems have opened a new window to overcome these problems.

Methods A polyelectrolyte carboxymethyl cellulose polymer as a magnetic nanocarrier was synthesized for enhancing delivery and uptake of doxorubicin in MCF7 breast cancer cells and decreasing the adverse toxic effects to healthy tissues.

Results The physicochemical properties of developed nanocarrier showed that it can be used in drug delivery purposes. The efficiency of the delivery system was assessed by loading and release studies. Besides, biological assays including protein-particle interaction, hemolysis assay, cytotoxicity study, cellular uptake, and apoptosis analysis were performed. All results persuaded us to investigate the cytotoxic effects of nanocarrier in an animal model by determining the biochemical parameters attributed to organ injuries, and hematoxylin and eosin (H&E) staining for histopathological manifestations. We observed that the nanocarrier has no toxic effect on healthy tissues, while, it is capable of reducing the toxic side effects of doxorubicin by more cellular internalization.

Conclusion Chemical characterizations and biological studies confirmed that developed nanocarrier with permanent cationic groups of imidazolium and anionic carboxylic acid groups is an effective candidate for anticancer drug delivery.

KEY WORDS enhanced drug delivery · doxorubicin toxicity MCF7 breast cancer cells · polyelectrolyte carboxymethyl cellulose

ABBREVIATIONS

ALT	Alanine aminotransferase
AST	Aspartate aminotransferase
CK	Creatine kinase
CMC	Carboxymethyl cellulose
Cr	Creatinine
DAPI	4′,6-diamidino-2-phenylindole
DDS	Drug delivery systems
DEE	Drug encapsulation efficiency
DLE	Drug loading efficiency
DLS	Dynamic light scattering
DOX	Doxorubicin
DSC	Differential scanning calorimetry
EDTA	Ethylenediaminetetraacetic acid
EDX	Energy-dispersive X-ray spectroscopy
EPR	Enhanced permeability and retention
FBS	Fetal bovine serum
FTIR	Fourier transform infrared PLGA
LDH	Lactate dehydrogenase
MDR	Multidrug resistance
MFI	Mean fluorescent intensity
MNPs	Magnetic nanoparticles

Vahid Shafiei-Irannejad and Mahdi Rahimi contributed equally to this work

✉ Bahman Yousefi
yousefib@tbzmed.ac.ir

1 Cellular and Molecular Research Center, Cellular and Molecular Medicine Institute, Urmia University of Medical Sciences, Urmia, Iran

2 Solid Tumor Research Center, Cellular and Molecular Medicine Institute Urmia University of Medical Sciences, Urmia, Iran

3 Drug Applied Research Center, Tabriz University of Medical Sciences, Tabriz, Iran

4 Aging Research Institute, Physical Medicine and Rehabilitation Research Centre, Tabriz University of Medical Sciences, Tabriz, Iran

5 Department of Organic and Biochemistry, Faculty of Chemistry University of Tabriz, Tabriz, Iran

6 Immunology Research Center, Tabriz University of Medical Sciences, Tabriz, Iran

MTT	3-(4, 5- dimethylthiazol-2-yl)-2, 5-diphe-nyltetrazolium bromide
P-gp	P-glycoprotein
RPMI-1640	Roswell Park Memorial Institute 1640 growth medium
SEM	Scanning electron microscopy
TEM	Transmission Electron Microscopy
VSM	Vibrating-sample magnetometer
Ur	Urea
XRD	X-ray diffraction

INTRODUCTION

Cancer as a disease has become the primary health concern in both developed and developing countries. Surgery, radiation therapy and chemotherapy are known as standard treatments for cancer. Chemotherapy is an essential tool for the treatment of many cancer types; however, there are some limitations for successful cancer treatment such as toxic adverse effects against healthy tissues, and resistance against anticancer compounds which is known as multidrug resistance (MDR) (1,2). To overcome these obstacles, one strategy is the use of nanotechnology to design and fabricate the drug delivery systems (DDS) for efficient and controlled delivery of multiple chemotherapeutic agents (3). The DDS results in a higher intracellular drug concentration in tumor cells by enhanced permeability and retention (EPR) effect as well as, minimizing the toxic side effects on normal cells (4,5). An ideal drug carrier should exhibit high stability and long lifetime in blood circulation, active or passive targeting abilities, and sustained and controlled delivery of drugs in the tumor environment (6,7). To date, different types of materials have been used for the purpose of drug delivery including micelles, liposomes, natural or synthetic polymers, dendrimers and magnetic nanoparticles (MNPs) (8,9). Dendrimers and multibranched polymers have attracted the attention of many researchers due to their capability in higher drug-loading capacity and release efficiencies. Polymers with branched moiety are very advantageous for the purpose of DDS due to increased drugs life-time in the systemic circulation, while, polymers without branched structures are easily removed by the renal system (10,11). Cellulose is a natural biopolymer which is widely used in medical applications due to its beneficial characteristics such as biodegradability, renewability, and non-toxicity (12). Carboxymethyl cellulose (CMC) is a cellulose-based polymer which has all biologic features mentioned for cellulose as well as the existence of active chemical groups such as hydroxyl and carboxylic acid which makes it ideal for drug delivery purposes and biotechnology applications (13). Moreover, the chemical groups in the surface of CMC can be modified with other desirable functional groups such as amine groups to achieve the maximum loading capacity for drugs as well as increasing the binding capacity of nanocarrier to target cells (14,15). Cationic nanoparticles can enter within cells in an energy-independent manner, escaping the traditional endocytosis route, which is known as direct translocation (16). Generally, it is found that cationic nanoparticles absorb or bind strongly to lipid bilayers, causing deformation of the membrane in favor of endocytosis (17). Therefore, by modification of CMC with moieties containing permanent cationic property, it can be derived easily inside the cell.

Unlike the linear and one-dimensional CMC polymer, branched and grafted CMC as the three dimensional polymers are expected to manifest multi-point interaction with other molecules resulting in enhanced binding ability (18). In recent years, magnetic nanoparticles (MNPs) such as Fe_3O_4 have gained particular attention in DDS. These nanoparticles can be efficiently conducted to target cells with the use of an external magnetic field. However, they need to be further surface coated with natural and biocompatible polymers to minimize the toxicity (19,20).

Doxorubicin (DOX), belonging to the anthracycline family of compounds, is a commonly used anticancer agent for the treatment of a wide range of malignancies such as lung cancer, breast cancer, and bladder carcinoma (21). However, toxic adverse effects on healthy tissues, especially cardiotoxicity and nephrotoxicity, is the main obstacle against DOX prescription which is mainly dependent on drug concentration (22,23). Another problem is the development of resistance (MDR) against DOX, in particular by overexpression of drug efflux proteins such as P-glycoprotein (P-gp) (24). Therefore, loading DOX into a safe nanocarrier seems to be a promising approach both to reduce toxic side effects and circumvent MDR.

In this study, we aimed to increase the efficiency of DOX by designing a branched CMC polyelectrolyte polymer with permanent cationic and anionic groups for surface modification of iron oxide nanoparticles in killing MCF7 cancer cells. Cationic branches of modified CMC could give the final nanocarrier a capability to attach the surface of the cancer cells and force the cell membranes to open doors for polyelectrolyte nanocarrier. The modified CMC could improve the stability of nanocarrier due to the presence of long and branched polyelectrolyte polymers. Furthermore, structural and physicochemical characteristics of the nanocarrier such as a chemical structure of the polymer, size and surface morphology of the particle, loading and encapsulation efficiencies, and biocompatibility of nanocarrier were analyzed. The cytotoxicity, cellular uptake, and apoptotic-inducing effects of DOX-loaded nanocarrier on MCF7 breast cancer cells were examined with multiple tests. Finally, the histopathologic and biochemical impacts of drug loaded nanocarrier on healthy organs after injection to mice model were studied.

EXPERIMENTAL SECTIONS

Animal and Ethics

Adult male mice (20–30 g) were purchased from Pasteur Institute of Iran (Tehran, Iran) and were kept at room temperature under daylight cycle of 12 h and had free access to tap water and rodents chow. All animal studies were carried out under approved protocols with the ethical committee of Tabriz University of Medical Sciences (National Institutes of Health Publication No. 85–23, revised 1996).

Materials

Some materials in this report were synthesized according to the previous literature and used as reagents. 1-methyl-3-(oxirane-2-ylmethyl)-1H-imidazol-3-ium chloride (ImIL) as an ionic-liquid based cyclic monomer was incorporated according to the Shojaei *et al.* (25). Sodium methoxide as a base was prepared according to the particular reaction between methanol and sodium which used freshly for activation of hydroxyl groups. All solvents were purchased from Merck Company (Germany) and purified according to the purification standard methods. SDS-PAGE gels were made with acrylamide and bisacrylamide (26). Milli-Q water system (Millipore S.A 67120, Molsheima, France). was used for purification of water and obtained deionized water was used in all experimental sections. Doxorubicin hydrochloride (85%) was purchased from Exir Nano Sina Co, Tehran, Iran. Sodium carboxymethyl cellulose, the degree of substitution (DS) 0.55–1.0, and viscosity 15,000 mPas/s (1% in H_2O, 25°C) were obtained from Nippon Paper Chemicals Co., Ltd., Japan. Other chemical reagents such as ferric chloride hexahydrate ($FeCl_3{\cdot}6H_2O$), ferrous chloride tetrahydrate ($FeCl_2{\cdot}4H_2O$), benzaldehyde (99%), and etc. were obtained from Merck Company. 4′,6- Diamidino-2-Phenylindole dihydrochloride (DAPI), and 3-(4, 5- dimethylthiazol-2-yl)-2, 5-diphe-nyltetrazolium bromide (MTT), propidium iodide (PI), ribonuclease A, and other biological reagents were purchased from Sigma-Aldrich Company (Germany). Fetal bovine serum (FBS, PAA Laboratories), trypsin, and Roswell Park Memorial Institute 1640 growth medium (RPMI) were purchased from Gibco™ (UK). Human breast cancer carcinoma MCF7 cell line was obtained from the Pasteur Institute of Iran, Tehran, Iran. Human red blood cells were obtained from the Iranian Blood Transfusion Institute (IBTI; Tehran, Iran) which stabilized with ethylenediaminetetraacetic acid (EDTA).

Instrumentation

The functional groups of the samples were determined using Fourier transform infrared (FTIR) (Bruker Tensor 270 spectrometer, Germany) spectroscopy at room temperature in the range of 500–4000 cm^{-1}. A laser scattering method (Zetasizer Nano ZS90, Malvern Instruments, Malvern, UK) was used to measure the mean size and surface charge of the nanoparticles at 25°C. The surface morphology and size of the samples were analyzed using scanning electron microscopy (SEM; FEG-SEM MIRA3 TESCAN, Czech Republic). For studying the magnetic properties of the nanoparticles, a vibrating-sample magnetometer (VSM; AGFM, Kashan, Iran) was used. X-ray diffraction (XRD) analysis was carried out with an X-ray 4 diffractometer (PHILIPS, PW1730, Netherlands), the power of 50 kV/50 mA and Cu Ka irradiation at room temperature. In all cases, Cu Kα radiation from a Cu X-ray tube was used. The samples were scanned in the Bragg angle (2θ) range of 10–80. Differential scanning calorimetry (DSC) was used to determine the thermal behavior of the polymers. The DSC test was performed using a Mettler DSC 821e (Mettler-Toledo, Switzerland) from 30 to 350°C, at a heating rate of 5°C min^{-1} under a flowing argon atmosphere. The thermogravimetric analysis (TGA) of samples were examined by thermal analyzer model TGA PT 1000 (Linseis, Germany) from 25 to 800°C at the rate of 10°C/min. The Transmission Electron Microscopy (TEM) analysis was used to show the size and core-shell characteristic of the sample by a Leo 906, Zeiss, Germany with operating at 100 kV. Before analysis, the suspension was dispersed using a probe-type ultrasonic generator (400 W) for 6 s, and the suspension was placed on a carbon-coated copper grid.

Preparation of Magnetic Nanocarrier (NC)

Development of Polyelectrlyte Carboxymethyl Cellulose (PIL-G-CMC)

Step 1- Activation of hydroxyl groups: To activate hydroxyl groups of CMC, sodium methoxide was used as a base. In this regard, 1.0 g CMC was added to 25 mL anhydrous DMF and dispersed for 5 min. Then, 3.0 g sodium methoxide was added to the above solution and stirred vigorously at 50°C for 2 h under N_2 atmosphere. Afterward, the solvent was evaporated under a vacuum condition.

Step 2 – Ring-opening polymerization of ImIL on CMC: The residue which obtained from step 1 was re-dispersed in 25 mL anhydrous DMF. Subsequently, excess amounts of ImIL solution were added gradually into the reaction suspension and stirred at 50°C. After 24 h, the suspension was centrifuged and precipitated in ethanol several times. Finally, PIL-*g*-CMC was vacuum dried at 50°C for overnight.

Preparation of PIL-G-CMC Coated Magnetic Nanoparticle (PIL-G-CMC/Fe_3O_4)

Step 1 – Preparation of magnetic nanoparticles (Fe_3O_4 NPs): In a three neck round bottom flask, 25 mL deionized water was added and 0.5 g $FeCl_3{\cdot}6H_2O$ and 1.25 g $FeCl_2{\cdot}4H_2O$ were also dissolved in the solution and stirred at 50°C for 30 min. The pH of the solution was increased up to 10 by adding gradually of ammonia solution (28%). The reaction mixture was stirred for 45 min, and the obtained Fe_3O_4 was isolated, washed and vacuum dried at 40°C for 16 h.

Step 2 – preparation of PIL-g-CMC/Fe_3O_4 NPs: 1 g of Fe_3O_4 NPs was dispersed in 50 mL of absolute methanol, and 1 mL of [3-(2,3-epoxypropoxy)propyl]-trimethoxysilane was added dropwise with vigorous stirring. The reaction was performed at 100°C for 6 h under an inert atmosphere, and a magnetic nanoparticle with a silica layer was obtained. For attaching PIL-*g*-CMC on the surface of the obtained nanoparticle, 0.5 g PIL-*g*-CMC was added to the reaction mixture and refluxed at 100°C for 48 h. Finally, PIL-g-CMC/Fe_3O_4 as a magnetic nanocarrier (NC) was collected by several centrifuging and washing with water and ethanol. The prepared nanocarrier was vacuum dried and used in the next step for DOX loading and release studies.

DOX Loading and Release Studies

Loading step: 10 mg of DOX was dissolved in 5 mL PBS solution and continuously shaken on a magnetic stirrer. For DOX loading purpose, 100 mg of prepared NC was added to the above solution and dispersed via probe sonicator. The obtained suspension was shaken for 24 h under dark condition (to prevent DOX decomposition by light). Then, the suspension was centrifuged at 5000 rpm for 5 min, and the supernatant was taken for measurement of unloaded DOX by UV-Vis spectrophotometer. Finally, the DOX-loaded nanocarrier (DOX-NC) was dried by freeze drying.

Releasing step: 10 mg DOX-NC was added to microtubes which categorized as follow: one group for pH 7.4 and the other group for pH 5.0 with three microtubes for each group. 2 mL PBS solution was added to each microtube and incubated at 37°C. At a particular time, the microtubes were centrifuged, and the supernatant was taken for determination of released DOX by UV-Vis spectrophotometer. Both drug encapsulation efficiency (DEE) and drug loading efficiency (DLE) were calculated according to the following equations:

$$DEE(\%) = \frac{Mass\ of\ DOX\ in\ NC}{Mass\ of\ feed\ DOX} \times 100 \quad (1)$$

$$DLE(\%) = \frac{Mass\ of\ DOX\ in\ NC}{Mass\ of\ NC} \times 100 \quad (2)$$

Hemolysis Assay

Blood compatibility of NC on human red blood cells was evaluated by hemolysis assay. In this regard, freshly human blood was received from IBTI, and the erythrocytes were collected by centrifuging the blood. The supernatant was taken out, and the erythrocytes were washed several times with PBS. Afterward, the precipitated human red blood cells (erythrocytes) were diluted ten times with PBS and treated with various concentrations of NC in triplicate. The treated samples were incubated at 37°C for 2 h. Finally, the samples were centrifuged at 4000 rpm for 5 min, and the supernatants were transferred to the 96-well plate for measuring lysis hemoglobin (at 570 nm by ELISA reader). The hemolysis rate was calculated by the following formula:

$$\text{Hemolysis Rate } (\%) = \frac{OD_{(sample)} - OD_{(-)}}{OD_{(+)} - OD_{(-)}} \times 100 \quad (3)$$

where $OD_{(sample)}$, $OD_{(-)}$, and $OD_{(+)}$ are the supernatant absorbance of the sample, negative and the positive control, respectively.

SDS-PAGE Assay

For evaluating the protein-particle interaction, SDS-PAGE staining assay was performed according to the following procedure. Briefly, 10 mg of NC was dispersed in PBS (pH 7.4) and incubated with human blood plasma (HBP) (200 µl) for 1 h. Then the unbounded proteins in the surface of the magnetic NC were removed by washing the NC several times with PBS. The bounded proteins were separated and with SDS-PAGE loading buffer. The proteins were further eluted with SDS-PAGE loading buffer and were loaded onto the 12% SDS-PAGE gel to study the proteins. As soon as the electrophoresis was over, the gel was stained with 0.25% Coomassie brilliant blue R-250 solution (at room temperature for 4 h) to visualize the protein lanes. Afterward, the gel was de-stained by incubation with a solution containing methanol (50 mL), water (40 mL), and acetic acid (10 mL) for 24 h and with slight

shaking and heating. A high-resolution photograph of the gel was taken with a scanner (HP Scanjet 3670).

Cell Culture

Human breast cancer (MCF7) cells were obtained from Pasteur Institute of Iran (Tehran, Iran) and cultured in RPMI-1640 containing 10% heat-inactivated fetal bovine serum (FBS), 100 unit/mL penicillin, 100 mg/mL streptomycin and incubated in 37°C with 5% CO_2. When cells reach 70% confluence, they were sub-cultured and used in all experiments (27).

MTT Assay

The *in-vitro* cytotoxicity of the blank NC, free DOX, and DOX-NC were assessed in MCF7 cells using MTT assay, as described previously. In brief, MCF7 cells were seeded in 96-well plates at the density of 10^4 cells per well and incubated at 37°C with 5% CO_2 for 24 h to allow the cells to attach to the bottom of the wells and grow. After 24 h, the medium was replaced with fresh medium containing different concentrations of free DOX, DOX-NC, and blank NC. Cells treated with new culture medium were considered as control group. After 48 h, the medium was removed and replaced with 200 µL fresh medium containing 100 µg mL^{-1} MTT powder and incubated for a further 4 h. Then the medium was withdrawn and 100 µL DMSO was added to dissolve the formazan crystals inside the cells. The absorbance of solubilized formazan was detected at 570 nm with the reference wavelength of 630 nm using ELISA plate reader (State Fax, 2100, Awareness Technology Inc., Palm City, FL, USA). The half-maximal inhibitory concentration (IC_{50}) of each treatment was also calculated.

Cellular Uptake by Fluorescent Microscopy and Flow Cytometry

To evaluate the internalization process of NC into the MCF7 cells, cellular uptake assay was performed using fluorescent microscopy imaging and flow cytometry. As DOX has fluorescent characteristics, it can be used as a marker for cellular uptake analysis of NC. After loading of DOX into NC utilizing the procedure described above, it was used in cellular uptake study. Briefly, MCF7 cells were cultured in 6-well plates at the density of 5×10^5 and incubated overnight to attach and grow. After 24 h, they were treated with DOX-NC at the concentration of IC_{50} and fresh medium as the negative control group. After cell incubation for 1 and 3 h, they were trypsinized, washed with PBS and subjected to flow cytometry analysis using FACScalibur flow-cytometer (Becton Dickinson Immunocytometry Systems, San Jose, CA, USA). For fluorescent microscopy, first cells were seeded in 6-well plates containing coverslips at the bottom of each well and incubated overnight allowing them to attach to the surface of coverslips and grow. After 24 h, cells were treated with DOX-NC and incubated for 1 and 2 h. Then the coverslips were fixed onto a glass microscope slides, and intracellular fluorescent emission associated with NC uptake was observed using a fluorescence microscope (Olympus microscope Bh2-RFCA, Japan).

Apoptosis Assay by DAPI Staining

To study the apoptotic effects of free DOX, DOX-NC and blank NC, 4′,6-diamidino-2-phenylindole (DAPI) staining assay were performed according to the following procedure. In brief, cells were seeded at 6-well plates containing coverslips at the density of 5×10^4 cells per well. After 24 h, the medium was replaced with fresh medium containing free DOX, DOX-NC, and blank NC at the concentration of IC_{50}. Cells receiving no treatment were considered as control group. Following 48 h, cells were washed three times with PBS and fixed with 4 wt% paraformaldehyde for 15 min at room temperature. Then, cells were washed with PBS and permeabilized with Triton X-100 (0.1% *w/v*) for 5 min. After cleaning the cells with PBS, they were stained with 300 ng/mL DAPI and incubated at dark for 15 min. Finally, the condensation and fragmented DNA of apoptotic cells were observed with a fluorescence microscope (Olympus microscope Bh2-RFCA, Japan).

In-Vivo Acute Toxicity Study

Five-week-old normal mice were randomly divided into three groups based on body weight. Each group contained five mice and treated with free DOX, DOX-NC, and NC. Mice treated with physiological serum were considered as control group. Both DOX and DOX-NC administration dosages were 10 mg per kg of body weight through tail vein injection. The body weight and physical changes of the mice were monitored every day. After four days of treatment, an appropriate amount of blood was collected, and the serum was isolated for measurement of some biochemical parameters including urea (Ur), creatinine (Cr), creatine kinase (CK), lactate dehydrogenase (LDH), alanine aminotransferase (ALT), and aspartate aminotransferase (AST). Three major organs including heart, liver, and kidneys were cut into serial 5 mm sections and fixed with 4% paraformaldehyde and stained with hematoxylin and eosin (H&E) for pathology analysis.

Statistical Analysis

All data were reported as mean ± SD of three independent experiments. One way analysis of variance (ANOVA) was used to show the significance between different groups.

Values lesser than 0.05 were considered as significant. Graphpad Prism 6.01 was used for data analysis.

RESULTS AND DISCUSSION

Preparation of Nanocarrier

PIL-*g*-CMC as a polymeric platform of our final nanocarrier was prepared based on ring opening polymerization of ImIL on the surface of CMC. In this regard, hydroxyl functional groups of the CMC backbone were deprotonated by sodium methoxide. Subsequently, ImIL as a cyclic monomer was added to the reaction mixture in which alkoxide (-O^-) terminal ends of CMC act as reactive centers and causing monomer rings open to form longer polymeric chains. The alkoxide (–O^-) as a nucleophile will attack atom carbon in ImIL cyclic monomer, thus releasing alkoxide. The newly formed alkoxide nucleophile will then attack the atom carbon in another ImIL monomer molecule, and the sequence would repeat until the polymer is formed (Fig. 1a-b). The formed grafted polymer has imidazolium ionic liquid branches which enable the final branching polymer with high stability in aqueous solutions.

Finally, magnetic nanoparticles (Fe_3O_4 NPs) with silica layer were coated with PIL-*g*-CMC with core-shell structure. It was expected to obtain a core-shell structure with a magnetic core and polymeric shell. Due to the presence of the silica layer with epoxy moiety on the surface of Fe_3O_4 NPs, PIL-*g*-CMC was attached to the magnetic base with epoxy functional groups as a linker. The polymeric outer layer can absorb the DOX as a model anticancer drug and use in the further *in-vitro* evaluation on MCF7 breast cancer cells and *in-vivo* histopathological analysis.

Characterization and Chemical Analysis

Before starting *in-vitro* biological evaluations, all materials which prepared in this study were characterized by several techniques including FTIR, XRD, DSC, SEM, EDX, TEM, VSM, DLS, and zeta potential analysis. All characterizations results confirmed that the synthesis and preparation of prepared samples were done successfully.

The FTIR spectra of CMC, PIL-*g*-CMC, PIL-*g*-CMC/Fe_3O_4 were taken to confirm their structure (Fig. 2a). In the FTIR spectrum of CMC, a broad absorption band was shown at 3467 cm^{-1} which is attributed to the stretching frequency of the –OH functional groups. The stretching vibration bands of C-H aliphatic group in CMC backbone appeared at 2923 cm^{-1}. As CMC has several carboxylate functional groups (-COO^-), a sharp peak around 1640 cm^{-1} also appeared. Also, C-O-C stretching vibration bond and

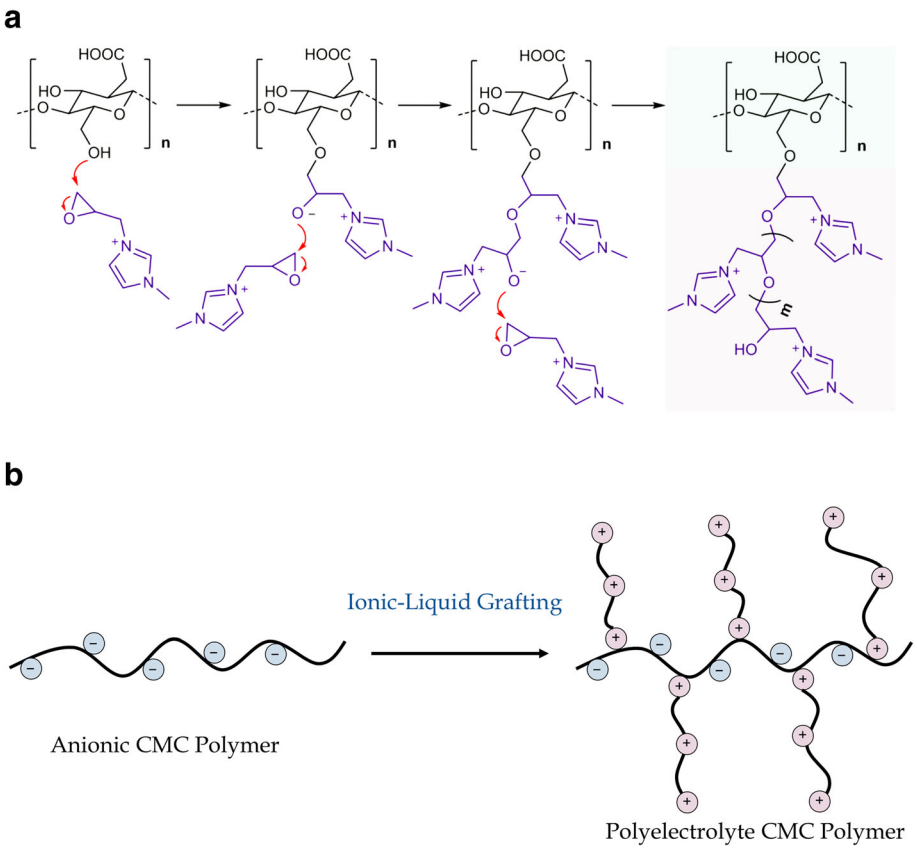

Fig. 1 (**a**) The mechanism for anionic ring-opening polymerization of ImIL on the surface of CMC to yield polyelectrolyte carboxymethyl cellulose (PIL-*g*-CMC) – (**b**) Anionic CMC modified to polyelectrolyte CMC by using ionic liquid monomer (ImIL).

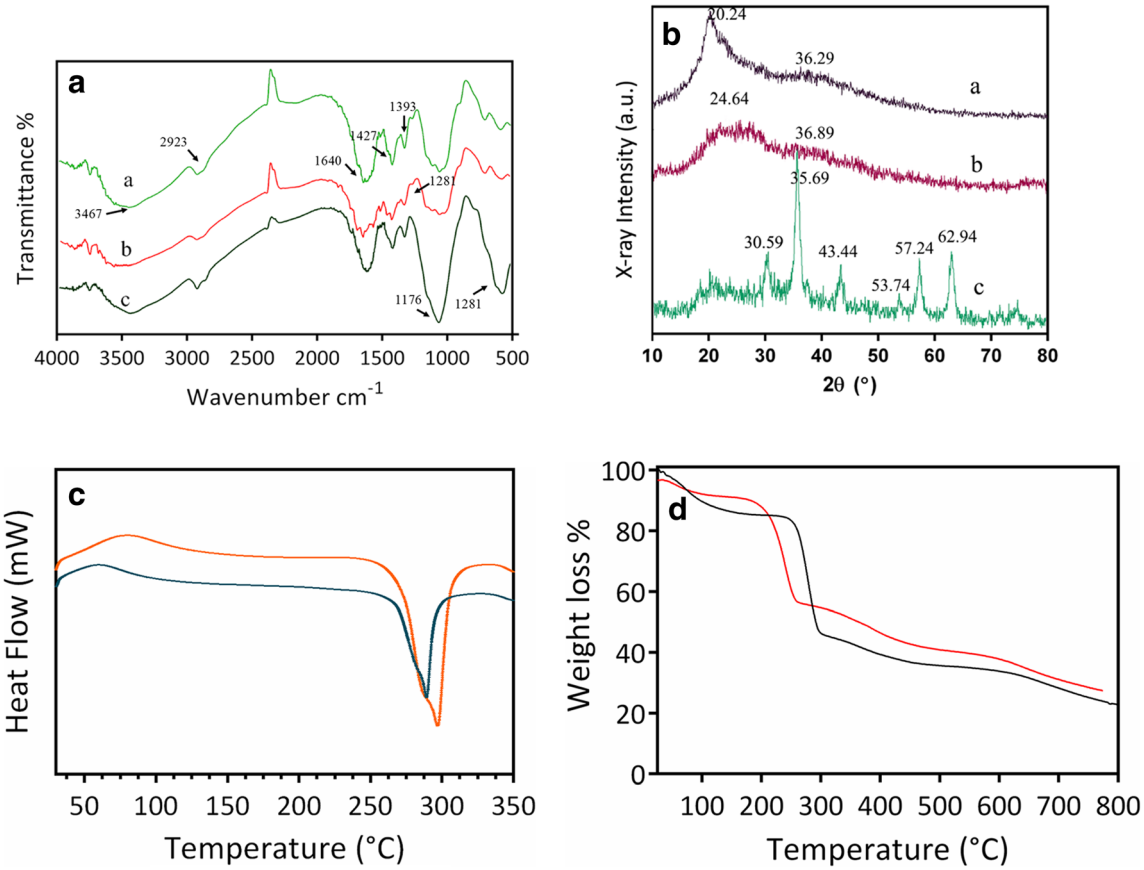

Fig. 2 (**a**) FTIR spectra of powder samples including CMC (a), PIL-*g*-CMC (b), and PIL-*g*-CMC/Fe_3O_4 (c) - (**b**) XRD diffractogram of powder samples including CMC (a), PIL-g-CMC (b), and PIL-*g*-CMC/Fe_3O_4 (c) – (**c**) Thermal behavior of CMC (a) and PIL-*g*-CMC (b) by DSC analysis (Endo up) from 30 to 350 C at a heating rate of 5°C min^{-1} under a flowing nitrogen atmosphere – (**d**) TGA graphs of CMC (a) and PIL-g-CMC (b) at the temperate range of 25 to 800°C.

deformation peak of C-O-H were seen at 1393, and 1427 cm^{-1}, respectively. PIL-*g*-CMC has the same functional groups such as –OH, C-H, -COO-, C-O-C, and C-O-H which have no significant shift in the FTIR spectrum. As expected, a new peak appeared at about 1281 which attributed to the C=N. This characteristic peak was related to the imidazolium groups on the polyionic liquid grafting on the CMC. After coating PIL-*g*-CMC on silica magnetic nanoparticles, two clear peaks were observed at 586 cm^{-1} for Fe-O and 1088 cm^{-1} for Si-O-Si bonds. The polymeric backbone characteristic peaks were also found in the FTIR spectrum of PIL-*g*-CMC/Fe_3O_4. All observations and results were validated in our preparation process.

The XRD diffractogram of powder samples including CMC, PIL-*g*-CMC and PIL-*g*-CMC/Fe_3O_4 were shown in Fig. 2b**.** The XRD pattern of CMC exhibits two different characteristic peaks at 20.24° and 36.29° with sharp and broad, respectively. The sharp peak was showed that the CMC has some crystallinity property and the broad peak is related to the amorphous part of CMC. After surface modification of CMC by polymerization of ImIL, PIL-*g*-CMC with amorphous structure was obtained. This could be explained by a rearrangement in the morphology of the CMC polymeric chain after grafting of PIL (28). By evaluation of XRD pattern, it was found that crystalline parts of CMC was also changed to the amorphous phase and the first CMC sharp peak was a boarder and transferred to 24.64°. Furthermore, the broad peak in CMC pattern was also exhibited in PIL-*g*-CMC. However, the peak is broader and appeared at 36.89°. The XRD pattern for PIL-*g*-CMC/Fe_3O_4 has several peaks in the range of 2θ about 10° to 80° which appeared at 2θ about 30.59°, 35.69°, 43.44°, 53.74°, 57.24° and 62.94° with relatively sharp. These peaks were attributed to the magnetic nanoparticles (Fe_3O_4 NPs) which were coated with the polymeric layer. To estimate the size of PIL-*g*-CMC/Fe_3O_4 as an NC, the Debye–Scherrer formula ($D = K\lambda/(\beta\cos\theta)$) was used. In the mentioned formula, the amounts of K (constant number for Cu-Ka; 0.9), λ (the X-ray wavelength for Cu-Ka; 0.15405 nm) and β (the peak width at half-maximum), and θ (the diffraction angle) were entered, and the amount of D (particle size) was calculated. After calculation with above-mentioned formula, the size of our NC has obtained 26.89 ± 2.36 nm.

To show and investigate the thermal behavior of CMC and PIL-*g*-CMC, DSC thermogram was recorded. As seen in Fig. 2c, an endothermic peak under 100°C was observed for

both CMC and PIL-*g*-CMC. This peak related to the presence of a solvent in the polymeric structure of both sample. The endothermic peak of PIL-g-CMC was disappeared earlier than CMC, due to the using organic solvent in the preparation process of PIL-*g*-CMC, whereas, the endothermic peak of CMC was observed about 100°C relating the adsorbed water. Besides, the DSC thermogram shows an exothermic peak at about 295°C for CMC and 288°C for PIL-*g*-CMC. These peaks are attributed to their melting point or oxidative degradation point of polymeric samples, indicating that thermal stability of PIL-*g*-CMC was decreased due to the grafting polyionic liquid branches.

TGA is a powerful technique of thermal analysis in which the mass of a sample is measured over time as the temperature changes. The TGA graphs of CMC and PIL-*g*-CMC was analyzed at the temperature range of 30 to 800°C at the rate of 10°C/min (Fig. 2d). The TGA graphs of CMC and PIL-g-CMC showed that the rate of weight loss is increased by increasing the temperature. A low weight loss was observed under 100°C in both graphs which attributed to the presence of water in the polymeric networks. The polymer decompositions temperature were found at 257 and 202°C for CMC and PIL-g-CMC, respectively. PIL-g-CMC started its decomposition earlier than CMC, and it is related to the presence of PIL side chains. However, the total weight loss of CMC and PIL-g-CMC are 77.20 and 68.92% at the range of 25 to 800°C.

To determine the presence of elements on the surface of samples, selected area energy dispersion spectrum (EDS) analysis was used which provides a semi-quantitative view of the elements. The weight percentages of elements (including carbon, C; oxygen, O; nitrogen, N; sodium, Na; iron, Fe; silicon, Si; and chlorine, Cl) were summarized in Fig. 3a. CMC has four main atoms including hydrogen, carbon, oxygen, sodium in its structure. EDS data illustrated 19.60%, 25.67%, and 51.43% weight percentage for Na, C, and O, respectively. Elemental analysis by EDS was also done for PIL-*g*-CMC to confirm the successful surface modification of CMC. Due to the presence of N and Cl atoms in the polymeric branch, it was expected that the weight percentages of N and Cl atoms were enhanced to 6.08% and 6.74%, respectively. Whereas, the weight percentage of other elements were decreased in comparison to CMC. Furthermore, silica coated magnetic nanoparticles were synthesized in the presence of polymeric solution (PIL-*g*-CMC/Fe_3O_4), and it was expected that Fe and Si atoms peaks appeared in EDS analysis graph. The atomic weight percentages of these atoms were 35.42% for Fe and 4.39% for Si atoms. In contrast, the atomic percentages of N, O, Cl, and Na were decreased in an amount significantly (CMC to PIL-*g*-CMC; N: 6.08 to 5.58% – O: 39.89 to 36.70% – Cl: 6.74 to 0.14% – Na: 11.34 to 1.37%). Decreasing atomic percentages of Cl and Na atoms in comparison to the others is attributed to their ionic form which could wash and exchange with other ions in the reaction processes. All EDS results confirmed the successful preparation and immobilization of PIL-*g*-CMC on the surface of silica coated magnetic nanoparticles.

DLS technique is used widely for determination of particle size in a liquid phase. Therefore, the size of our NC was analyzed with this technique in a PBS solution (pH = 7.4) (Fig. 3b). However, some factors (such as the concentration of particle suspension, scattering angle, and shape anisotropy of nanoparticles) can influence the determination of the particle size (29). Prepared NC was dispersed in PBS (pH 7.4), and the particle size distribution was measured by DLS. The result showed that NC has about 200 nm size. The high observed particle size of is corresponded to a concentration of the sample, which was tested under aqueous solution. Whereas, the accurate size of particles was determined and confirmed by SEM and XRD. The overall surface charge of NC in PBS solution (pH 7.4) was about −17 mV which it is related to the presence of –COOH, and –OH on the surface of polymeric backbone and silica-coated magnetic nanoparticles that alter to ionic form in this pH (-COO^- and $–O^-$).

Drug carriers with magnetic features have been widely used in DDS, because of efficiently conducting to the target cancer tissues by an external magnetic field. Magnetic nanocarrier with good magnetization value more than 10 emu g^{-1} can be used in biomedical applications (30). In this regard, a vibrating sample magnetometer (VSM) was used for measuring magnetic properties at 298 K in a field of 10 kOe. As seen in Fig. 3c, prepared NC has about 52 emu g^{-1} magnetization value with superparamagnetic properties. Bulk magnetic nanoparticles (Fe_3O_4 NPs) has more magnetization value which is attributed to their bare structure in compared to the core-shell structure of the NC. Therefore, the obtained amount of magnetization afforded by NC is suitable for biomedical applications and drug delivery systems.

The surface morphology of samples was studied by SEM analysis which is presented in Fig. 4a. As seen, the surface of CMC is smooth with low crystalline parts. It is clear that the morphological structure of the CMC changes with surface modification. Therefore, it was expected that the addition of ImIL seems to cause changes in the morphological properties. The observation is in agreement with the general concept that ImIL polymerized at the surface of the CMC and was altered to the specific shape. As enlarging the image, many bulges are clearly seen and modified CMC change to the rough surface with spherical like shape on the surface which exhibits a branched surface to facilitate the attachment of drug molecules onto the surface. Furthermore, the crystalline part of PIL-*g*-CMC was also altered. After surface modification of silica coated magnetic nanoparticle with PIL-*g*-CMC, spherical particles with nanosize 39.23 ± 8.41 nm were formed. All observations confirmed that surface modification processes were done successfully.

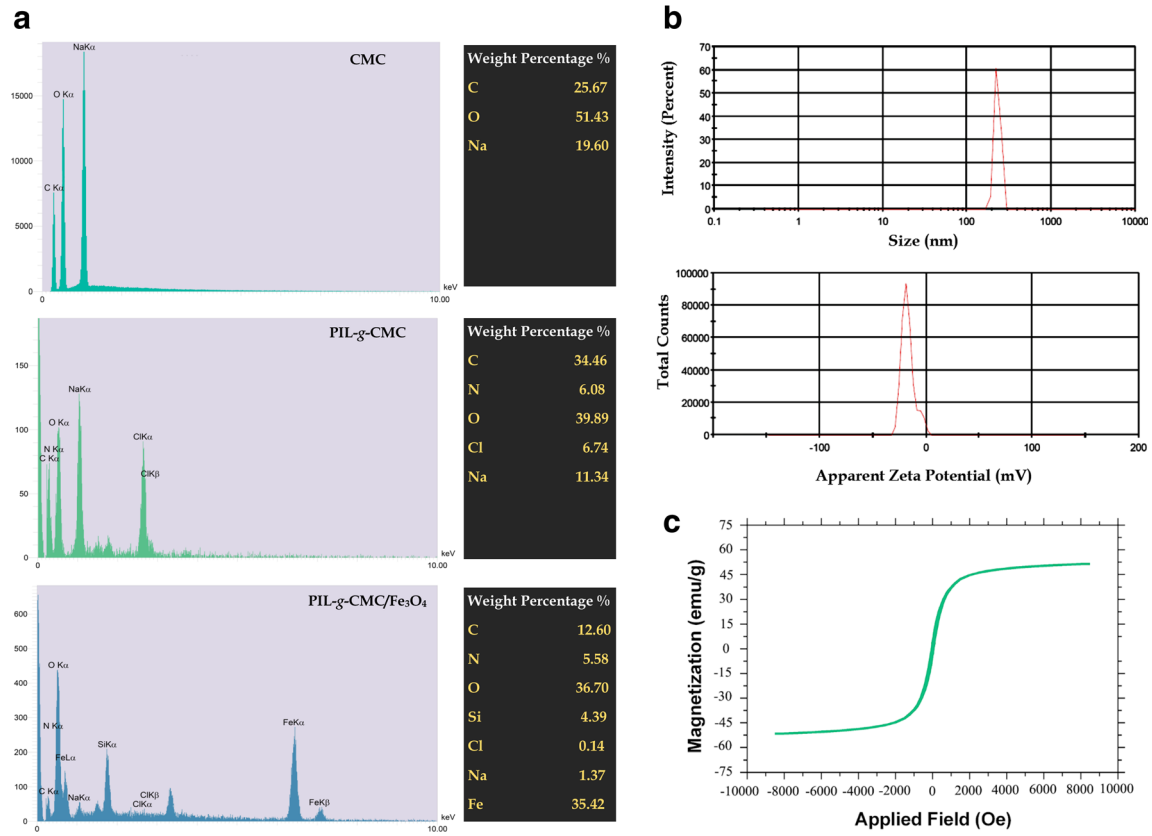

Fig. 3 **(A)** The EDS analysis diagrams and data (weight percentage %) of CMC, PIL-*g*-CMC, PIL-*g*-CMC/Fe_3O_4 – **(B)** DLS (upper) and zeta potential (bottom) analysis of NC in PBS solution (pH 7.4) – (**C**) Magnetic properties of PIL-*g*-CMC/Fe_3O_4 (NC) with magnetization values of 52 emu g^{-1}.

TEM is another powerful instrument with good capability to determine several features such as the crystal structure and functions in the structure like dislocations and grain boundaries. As seen in Fig. 4b, Fe_3O_4 nanoparticles not only had the been stabilized by wrapping PIL-*g*-CMC in their surface to prevent them from coagulation, but the affinity of the aggregation was also observed. The TEM image was also showed that the morphology of PIL-*g*-CMC/Fe_3O_4 was nearly spherical with a magnetic core polymeric shell. By enlarging the picture, it was found that the shell layer has a low thickness about 3 nm in comparison to the magnetic core with 20 nm diameter.

Biocompatibility of NC on Human Red Blood Cells

Fe_3O_4 nanoparticles (MNPs) have good potentials in biomedical application due to their magnetic properties. Therefore, blood compatibility should be evaluated for nanoparticles due to their interaction with red blood cells after intravenous injection to the body. To assess the interaction of medical devices with blood, some biological analysis can be performed including thrombosis, coagulation, platelets, hematology, and hemolysis assay should be investigated (31). Hemolysis is the breakdown or destruction of red blood cells containing hemoglobin (oxygen-carrying pigment) which is distributed into the surrounding medium before their average lifespan is up. Rupturing red blood cells (erythrocytes) leads to anemia, jaundice and renal failure (32). In this regard, to assess the impact of NC on erythrocytes, hemolysis assay was done for measuring released hemoglobin by UV-Vis spectrophotometric after treating with various concentrations of NC (3200, 1600, 800, 400, 200, 100, 50, 25, 12.5, 6.25, and 3.12 μg mL^{-1}) (Fig. 5a). The hemolysis assay results showed that the hemolytic activity of NC has dose-dependent property. As seen in Fig. 5b, water as a positive control caused ~100% hemolysis while NC only led to ~3.33% hemolysis at the concentration of 3200 μg mL^{-1}. The erythrocyte sedimentation rate (ESR) is the rate of red blood cells sedimentation in a period of one hour. The ESR test is known as a non-specific measure of inflammation and hematology test. In this regard, blood was placed in a Westergren tube (upright tube) containing citrate as an anticoagulant agent, and the rate of sedimentation of red blood cells was measured in mm at the end of one hour. As seen in Fig. 5c, tubes containing blood treated with NC has the same amount of ESR value in comparison to control. The results showed that the NC has no effect on the surface charge

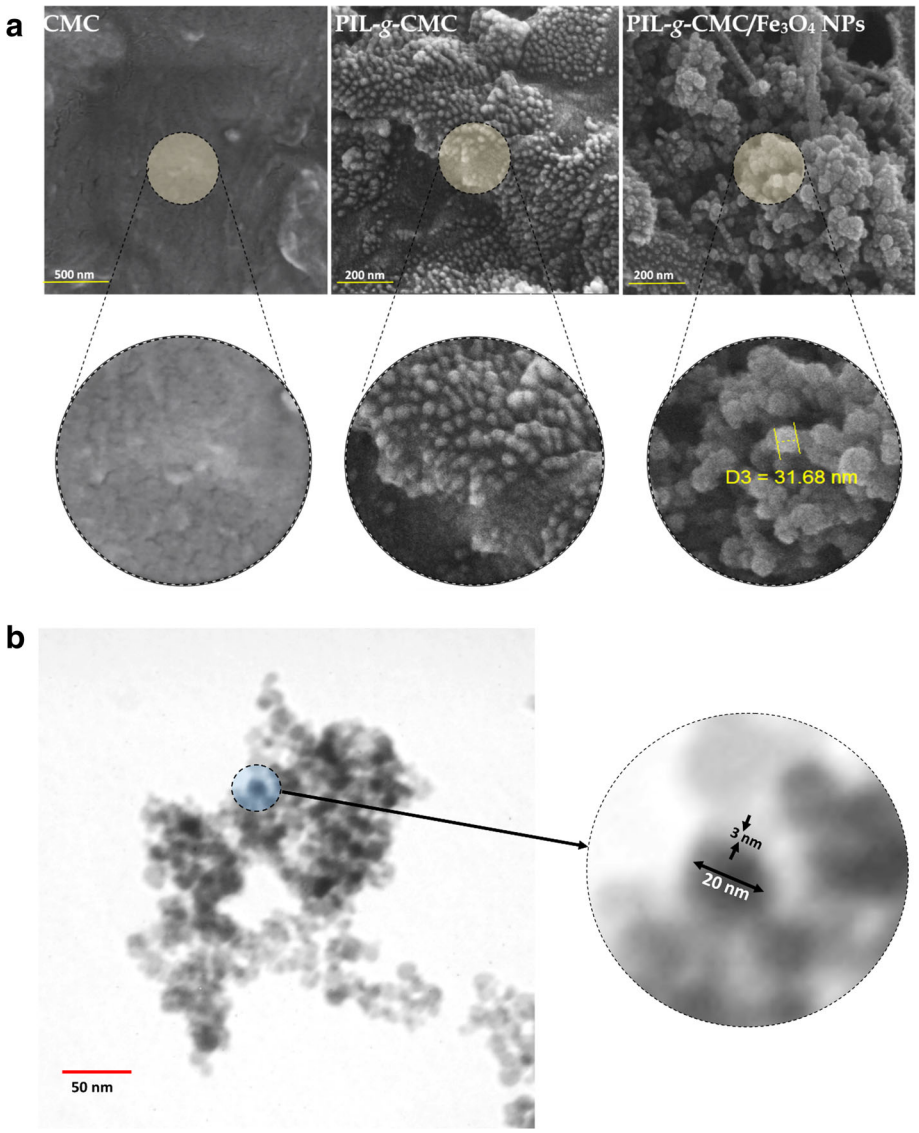

Fig. 4 (**a**) Surface morphology and size evaluation of sample by SEM analysis. The scale of CMC, PIL-*g*-CMC, and PIL-*g*-CMC/Fe_3O_4 are 2 μm, 500 nm, and 200 nm, respectively. (**b**) TEM images of PIL-*g*-CMC/Fe_3O_4 with core-shell structure (thin layer of PIL-*g*-CMC with a thickness of about 3 nm and a diameter of 20 nm magnetic nanoparticle core analyzed by Image J software).

of red blood cells and therefore the rate of sedimentation didn't change.

Stability of Nanocarrier

The determination of nanoparticles dispersity is a critical step in understanding their behavior in water (33). For this reason, the stability of NC was evaluated to better understand the aggregation and stability of NC in aqueous solution and facilitate the prediction of their fate in the physiological condition. To explore the stability of NC, PBS solution with pH = 7.4 as a simulation for physiological and blood circulation conditions (pH = 7.4; 37°C) was used (Fig. 6a). A relatively high dosage of NC was added gradually into the container and the changes in precipitation with time were monitored. After continuous addition of NC into the vessel and mild shaking, the color of the suspension was changed to light brown. The results confirmed that the suspension has excellent stability with low sedimentation rate in which the aggregation can be easily broken down by sonication or stirring. In addition, when nanocarrier suspension was kept in the PBS, it showed excellent stability in comparison to bare Fe_3O_4 NPs at the same concentration.

Protein-Particle Interaction Evaluation by SDS-PAGE Assay

One of the crucial issues in the field of nanomedicine and DDS is the interaction of particles with blood components. Therefore, it is essential to study and predict the nanostructured materials behavior in biological fluids prior to *in-vivo* applications. In biological fluids, nanoparticles adsorb various types of macromolecules such as lipids and proteins on their surface. The protein layer bounded on the surface of particles is named as the protein corona. The composition of protein corona on the surface of particles is determined by several

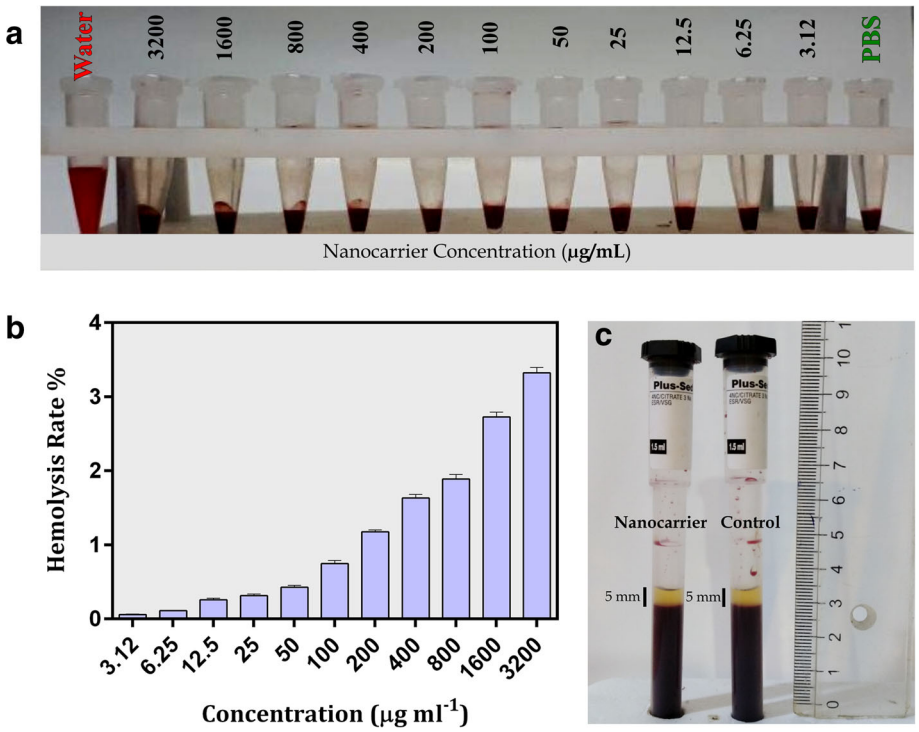

Fig. 5 (**a**) Optical image of the presence of hemoglobin in the red blood cells treated with various concentrations of NC and (**b**) hemolysis rate (%) in *versus* level of NC ($\mu g\ mL^{-1}$) - **(c)** The erythrocytes sedimentation rate (ESR) of blood treated with NC and blood with no treatment set as a control.

factors such as size, surface morphology, and charge, functional groups and type of nanomaterial. In this study, human blood plasma was used as a control to know which proteins are attached to the surface of NC after incubation for 1 h (Fig. 6b). Furthermore, a protein ladder with a molecular weight ranging from 25 to 250 kDa was used in decreasing

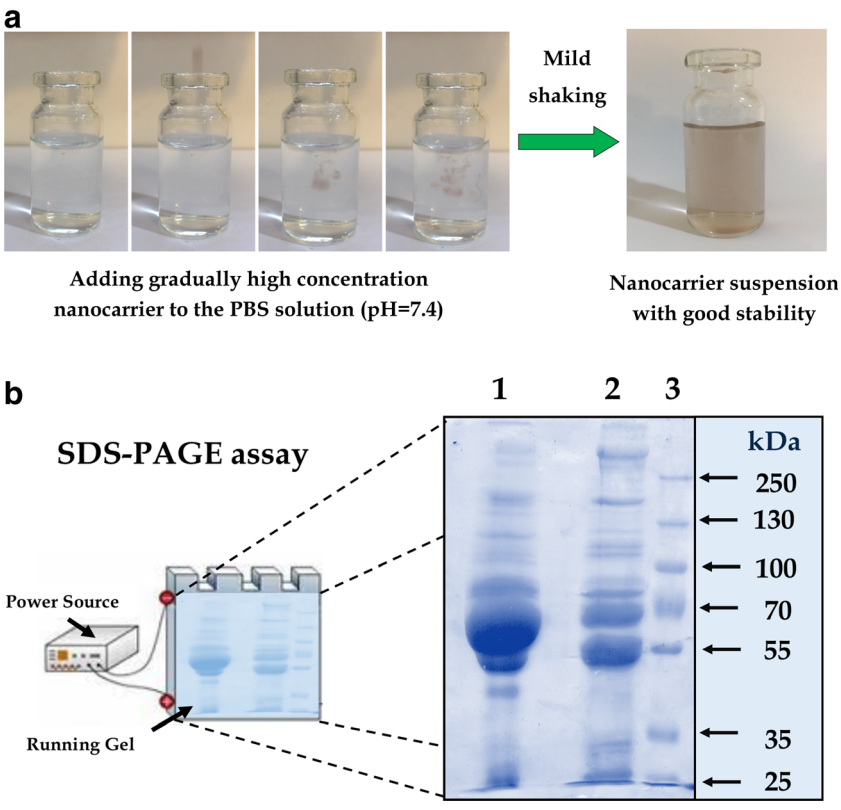

Fig. 6 (**a**) Stability and easily dispersion of NC in aqueous solution – (**b**) Protein-particle interaction of prepared NC with human plasma proteins by SDS-PAGE assay. Human plasma as a control (lane 1), attached proteins to the surface of NC (lane 2), and ladder (lane 3).

molecular weight order (Lane 3). Masking NC with plasma proteins can increase their biocompatibility and help them evade from recognition and elimination with the reticuloendothelial system (RES). Moreover, several types of proteins are present in corona which have receptors on the surface of many types of cancer cells including breast cancer that may increase the receptor-mediated internalization of the NC (34).

In-Vitro DOX Loading and Release Studies

High drug-loading on drug carriers has a essential role in the field of nano-particulate drug-delivery systems which is an effective way for treatment of cancer cells. Therefore, we have designed a nano-drug carrier with the capability of high DOX loading and encapsulation efficiencies. After calculation of both parameters with formulas 1 and 2, the amounts of loading and encapsulation efficiencies were obtained 8.52 ± 3.98% and 85.26 ± 5.22%, respectively. Due to the presence of carboxylate functional groups (-COOH) on the PIL-*g*-CMC and amine functional groups (-NH_2) on DOX, in physiological condition (pH 7.4), -COOH and -NH_2 change their structure to ionic form (-COO^- and –NH_3^+) and bind with each other via hydrogen bonding and ionic interaction. To simulate the DOX release in both physiological and cancerous tissues conditions, DOX-NC was dispersed in PBS solution in both pH 7.4 and 5.0 and release profile was evaluated for 130 h (Fig. 7a). As mentioned before, DOX was loaded on the surface of final NC with strong bonding, and it was expected that DOX release in pH 7.4 value passed up. However, DOX release in pH 5.0 showed initial burst release in first hours and sustained release after 10 h in which about 80% of loaded DOX was released after 130 h evaluation.

Cytotoxicity Assay

The cytotoxic effects of different concentrations of free DOX, DOX-NC, and blank NC on MCF7 cells were determined by MTT assay. As seen in Fig. 7b, no substantial cytotoxicity was

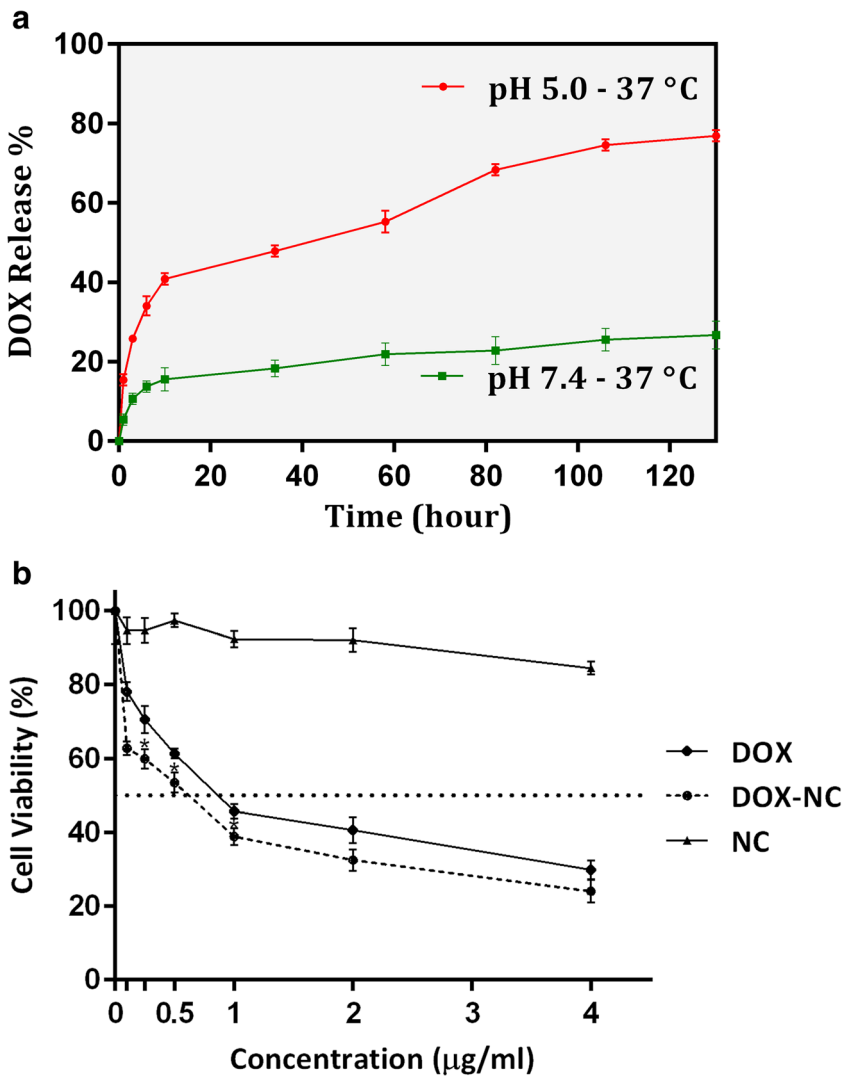

Fig. 7 (**a**) Cumulative release profile of DOX under physiological (pH = 7.4) and tumor tissue conditions (pH = 5.0) at 37°C for 130 h - (**b**) The cytotoxicity of free DOX, DOX-NC, and blank NC on MCF7 cells after 48 h. Each point represents the Mean ± SD of three independent experiments. *$p < 0.05$ vs control.

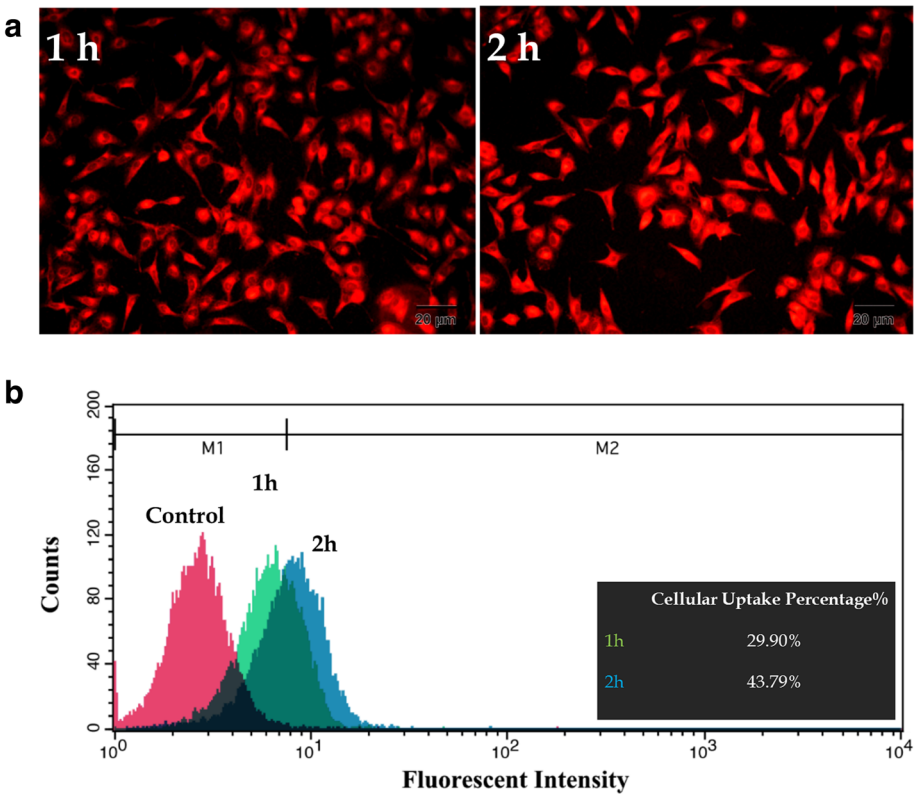

Fig. 8 (**a**) DOX-NC uptake into the MCF7 cells after 1 and 2 h treatment time with fluorescent microscopy (upper images) and without fluorescent microscopy (bottom pictures). (**b**) Flow cytometry analysis of cellular uptake of DOX-NC by MCF7 cells for 1 and 2 h. Cells treated without DOX-NC considered as control group – (**c**) Fluorescent microscopic images of DAPI stained cells following 48 h treatment with fresh medium (control), NC, free DOX (DOX), and DOX-NC.

observed for blank NC at concentrations of 10 times greater than free DOX, and DOX-NC which is comparable to control group, suggesting that our NC is safe for use in DDS in further *in-vivo* studies. To compare the cytotoxic effects of free DOX and DOX-NC, same concentrations were treated in MCF7 cells for 48 h. Results showed that the viability of the cells in both groups decreased in a dose-dependent manner. The IC_{50} of DOX in both groups was calculated as 0.956 μg/mL and 0.465 μg/mL for DOX and DOX-NC, respectively. In comparison with free drug, higher cytotoxicity was observed in DOX-NC which is confirmed by a shift to left in cytotoxicity profile, indicating the decreased IC_{50} and enhanced efficiency of DOX in nanostructured form.

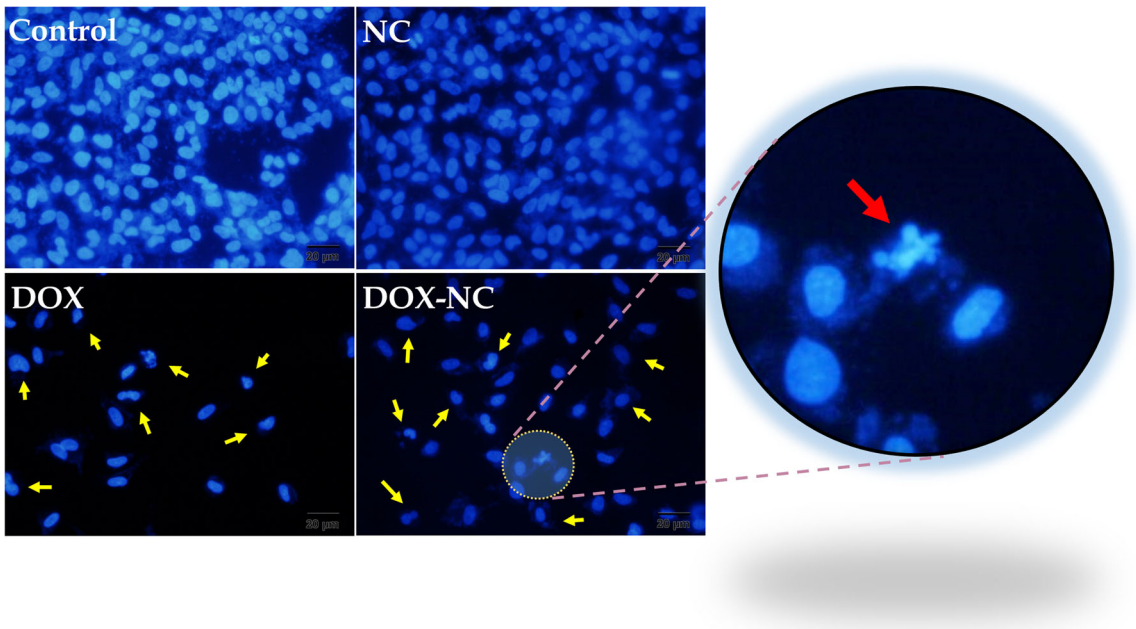

Fig. 9 Fluorescent microscopic images of DAPI stained cells following 48 h treatment with fresh medium (control), NC, free DOX, and DOX-NC.

Table I Biochemical Parameters in Mice After Treatment with Various Samples. Mice Treated with Physiological Serum Considered as a Control

	LDH (IU/L)	CK (IU/L)	BUN (mg/dL)	Cr (mg/dL)	ALT (IU/L)	AST (IU/L)
Control	257 ± 16	315 ± 21	14.2 ± 1.5	0.72 ± 0.04	42 ± 8	64 ± 11
NC	281 ± 11	374 ± 13	12.6 ± 2.3	0.77 ± 0.06	51 ± 12	58 ± 14
DOX	2476 ± 124	3428 ± 157	53.7 ± 8.1	2.1 ± 0.13	157 ± 24	183 ± 25
DOX-NC	922 ± 38	863 ± 47	27.5 ± 6.3	1.4 ± 0.09	98 ± 17	107 ± 19

Intracellular Uptake Study

The intracellular uptake of the NC into the cells was evaluated using qualitative fluorescence microscopy and quantitative flow-cytometry. In this analysis, the fluorescent feature of DOX was used as a marker for studying the internalization of the NC after 1 and 2 h treatment. As observed in Fig. 8a, DOX-NC internalized inside the cells in the uptake process and had different fluorescent intensity indicating that the internalization process was increased by passing the time. To confirm this analysis, mean fluorescence intensity (MFI) associated with intracellular DOX accumulation as an indicator of NC uptake was measured using flow cytometry (Fig. 8b). Results showed that the quantitative percentage of NC uptake was 29.90% for 1 h and 43.79% for 2 h. Both uptake analyses were validated that NC could internalize efficiently to the cells, suggesting that NC has a good capability to permeate into the cells and release loaded DOX. Results also confirmed that the modified CMC with two cationic and anionic electrolyte on the surface of the NC might improve the cellular uptake process by attaching to the cell membrane and opening doors for penetrating NC into the cells (16).

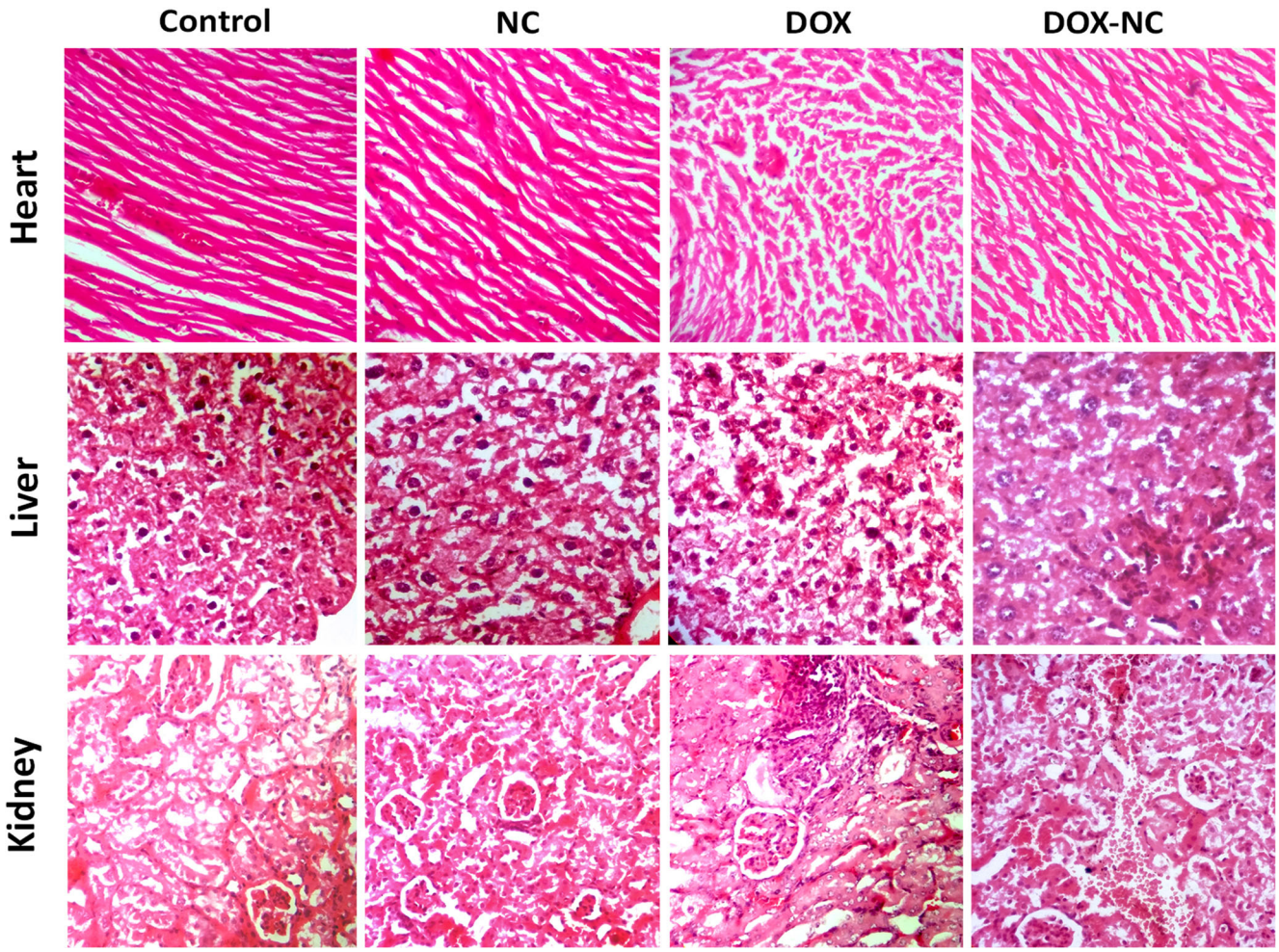

Fig. 10 Hematoxylin and eosin (H&E) staining of heart, liver, and kidney after treatment of mice with NC, DOX, and DOX-NC. Mice treated with physiological serum considered as a control.

Apoptotic Effect Evaluation Bay DAPI Staining

The morphology of chromatin and its condensation is a good indicator of healthy, apoptotic and necrotic cells. In this study, the apoptotic-inducing effect of treating with various samples in MCF7 cells was analyzed by DAPI staining for 48 h. Fluorescent microscopy images showed that untreated control groups had no change in nuclei of the cells with homogeneously stained and equally distributed in the nucleolus. Similarly, cells treated with NC didn't show significant morphological changes in cellular nuclei, suggesting that our NC is safe to use in *in-vivo* applications which are previously shown in MTT assay. As seen in Fig. 9, apoptotic cells are observed in cells treated with DOX and DOX-NC which is confirmed by chromatin fragmentation. However, cells treated with DOX-NC showed more changes in nuclei in comparison to free DOX. Furthermore, in the same microscopic field at all groups, lower cells are observed in DOX and DOX-NC treated cells, indicating that they could arrest cell proliferation in comparison to untreated cells and blank NC treated cells.

In-Vivo Toxicity Evaluation

One of the significant challenges toward successful cancer chemotherapy is toxic side effects against healthy tissues. Therefore, reducing adverse toxic effects of chemotherapeutic agents in healthy tissues is an outstanding deal. DOX is a potent anticancer agent which is widely used for the treatment of various types of tumor cells, but treatment with this drug is accompanied with severe toxic effects to healthy tissues such as heart, liver, and kidney which is directly associated with drug concentration (35). To overcome this problem, one strategy is to use nanotechnology and drug delivery systems for carrying chemotherapeutic agents in blood circulation. As observed in the results of cytotoxicity study, treatment with DOX-loaded nanocarrier significantly decreased the IC_{50} value of DOX when compared to free DOX, indicating that the synthesized nanocarrier is capable of declining adverse toxic effects on healthy tissues, with no impact on its efficiency on cancer cells. To investigate the effects of synthesized nanocarrier on healthy tissues, free DOX, NC, and DOX-NC were injected to mice, and biochemical indicators of tissue injury and histopathological changes of heart, liver and kidney in mice were analyzed. Four days after injection of free DOX, DOX-NC, blank NC, and physiological serum (as control group), the toxic effects against organs were evaluated by determination of serum levels of LDH, AST, ALT, BUN, and Cr. As seen in Table I, the serum levels of LDH (indicators of heart injury), ALT and AST (signs of liver injury), BUN and Cr (indicators of kidney failure) were significantly increased in mice treated with free DOX in comparison with control group and mice treated with DOX-NC. In addition, no significant changes in biochemical markers were observed for blank NC, which is comparable to the control group, indicating that the NC is safe and has no toxic effects. Furthermore, the H&E staining of heart, liver and kidney tissues were performed after treatment with NC, free DOX and DOX-NC and were then examined with a light microscope. As seen in Fig. 10, no histological changes were observed for the control group, and blank NC treated group. However, treatment with DOX led to extensive pathological damage at all three organs. Furthermore, animals treated with DOX-NC, showed mild histological changes in comparison to free DOX, indicating that the NC was successful in decreasing the toxic effects of DOX in the heart, liver, and kidney.

CONCLUSION

To enhance the efficiency of DOX, a novel CMC based nanocarrier with polyelectrolyte property was designed and used in the treatment of MCF7 breast cancer cells. Firstly, a multifunctional polyionic liquid grafted CMC was intended to enhance the binding capacity for drug sites with 3D architecture and improve the attachment efficacy of modified CMC to the cancer cells due to its cationic polyelectrolyte section. All physicochemical characterizations validated our polymer modification. In the next step, DOX was loaded on the nanocarrier with high loading and encapsulation efficiencies. The *in-vitro* release profile showed that the nanocarrier has pH-responsive property. Biocompatibility of nanocarrier was confirmed by hemolysis assay and erythrocytes sedimentation rate analysis. Furthermore, SDS-PAGE staining was done to show the protein-particle interaction in simulated blood circulation systems. Cellular uptake studies were also performed to demonstrate the high internalization of nanocarrier inside the cells. To evaluate the apoptotic effect of DOX-NC in comparison to DOX, DAPI staining was used to show DNA fragmentation as an indicator for cellular apoptosis. The cytotoxicity study revealed that our NC could decrease the IC_{50} of DOX in MCF7 cells, indicating that the NC decrease the effective dose of DOX with no effect on its efficiency. Furthermore, no toxic effects for blank NC were observed which was further confirmed in animal studies. These results persuaded us to use this nanocarrier for other diagnostic and therapeutic biomedical applications.

ACKNOWLEDGMENTS AND DISCLOSURES

We thank the Drug Applied Research Centre (DARC), Aging Research Institute, Physical Medicine and Rehabilitation Research Centre, Clinical Research Development Unit, Shohada Hospital, Tabriz University of Medical Sciences,

Tabriz, Iran and Cellular and Molecular Research Centre, Cellular and Molecular Medicine Institute, Urmia University of Medical Sciences, Urmia, Iran. The authors report no conflicts of interest.

REFERENCES

1. Gottesman MM, Lavi O, Hall MD, Gillet JP. Toward a better understanding of the complexity of Cancer drug resistance. Annu Rev Pharmacol Toxicol. 2016;56:85–102.
2. Shafiei-Irannejad V, Samadi N, Salehi R, Yousefi B, Zarghami N. New insights into antidiabetic drugs: possible applications in Cancer treatment. Chem Biol Drug Des. 2017;90:1056–66.
3. Holohan C, Van Schaeybroeck S, Longley DB, Johnston PG. Cancer drug resistance: an evolving paradigm. Nat Rev Cancer. 2013;13(10):714–26.
4. Maeda H, Nakamura H, Fang J. The EPR effect for macromolecular drug delivery to solid tumors: improvement of tumor uptake, lowering of systemic toxicity, and distinct tumor imaging in vivo. Adv Drug Deliv Rev. 2013;65(1):71–9.
5. Liu Y, Fang J, Kim Y-J, Wong MK, Wang P. Codelivery of doxorubicin and paclitaxel by cross-linked multilamellar liposome enables synergistic antitumor activity. Mol Pharm. 2014;11(5):1651–61.
6. Jahanban-Esfahlan R, de la Guardia M, Ahmadi D, Yousefi B. Modulating tumor hypoxia by nanomedicine for effective cancer therapy. J Cell Physiol. 2018;233(3):2019–31.
7. Rahimi M, Shojaei S, Safa KD, Ghasemi Z, Salehi R, Yousefi B, *et al.* Biocompatible magnetic tris (2-aminoethyl) amine functionalized nanocrystalline cellulose as a novel nanocarrier for anticancer drug delivery of methotrexate. New J Chem. 2017;41(5):2160–8.
8. Zhang P, Li J, Ghazwani M, Zhao W, Huang Y, Zhang X, *et al.* Effective co-delivery of doxorubicin and dasatinib using a PEG-Fmoc nanocarrier for combination cancer chemotherapy. Biomaterials. 2015;67:104–14.
9. Rahimi M, Safa KD, Salehi R. Co-delivery of doxorubicin and methotrexate by dendritic chitosan-g-mPEG as a magnetic nanocarrier for multi-drug delivery in combination chemotherapy. Polym Chem. 2017;8(47):7333–50.
10. Hennink W, Park K. The influence of polymer topology on pharmacokinetics. Elsevier; 2009.
11. Rahimi M, Shafiei-Irannejad V, Safa KD, Salehi R. Multi-branched ionic liquid-chitosan as a smart and biocompatible nano-vehicle for combination chemotherapy with stealth and targeted properties. Carbohydr Polym. 2018;196:299–312.
12. Moon RJ, Martini A, Nairn J, Simonsen J, Youngblood J. Cellulose nanomaterials review: structure, properties and nanocomposites. Chem Soc Rev. 2011;40(7):3941–94.
13. Aouada FA, de Moura MR, Orts WJ, Mattoso LH. Preparation and characterization of novel micro- and nanocomposite hydrogels containing cellulosic fibrils. J Agric Food Chem. 2011;59(17):9433–42.
14. Elumalai R, Patil S, Maliyakkal N, Rangarajan A, Kondaiah P, Raichur AM. Protamine-carboxymethyl cellulose magnetic nanocapsules for enhanced delivery of anticancer drugs against drug resistant cancers. Nanomed: Nanotechnol, Biol Med. 2015;11(4):969–81.
15. Dai L, Yang T, He J, Deng L, Liu J, Wang L, *et al.* Cellulose-graft-poly (l-lactic acid) nanoparticles for efficient delivery of anti-cancer drugs. J Mater Chem B. 2014;2(39):6749–57.
16. Lin J, Alexander-Katz A. Cell membranes open "doors" for cationic nanoparticles/biomolecules: insights into uptake kinetics. ACS Nano. 2013;7(12):10799–808.
17. Lin J, Zhang H, Chen Z, Zheng Y. Penetration of lipid membranes by gold nanoparticles: insights into cellular uptake, cytotoxicity, and their relationship. ACS Nano. 2010;4(9):5421–9.
18. Wei L, Chen C, Hou Z, Wei H. Poly (acrylic acid sodium) grafted carboxymethyl cellulose as a high performance polymer binder for silicon anode in lithium ion batteries. Sci Rep. 2016;6:19583.
19. Zhang Y, Kohler N, Zhang M. Surface modification of superparamagnetic magnetite nanoparticles and their intracellular uptake. Biomaterials. 2002;23(7):1553–61.
20. Rahimi M, Safa KD, Alizadeh E, Salehi R. Dendritic chitosan as a magnetic and biocompatible nanocarrier for the simultaneous delivery of doxorubicin and methotrexate to MCF-7 cell line. New J Chem. 2017;41(8):3177–89.
21. Azimi A, Majidinia M, Shafiei-Irannejad V, Jahanban-Esfahlan R, Ahmadi Y, Karimian A, *et al.* Suppression of p53R2 gene expression with specific siRNA sensitizes HepG2 cells to doxorubicin. Gene. 2018;642:249–55.
22. Shafiei-Irannejad V, Samadi N, Yousefi B, Salehi R, Velaei K, Zarghami N. Metformin enhances doxorubicin sensitivity via inhibition of doxorubicin efflux in P-gp-overexpressing MCF-7 cells. Chem Biol Drug Des. 2018;91(1):269–76.
23. Yousefi B, Samadi N, Baradaran B, Rameshknia V, Shafiei-Irannejad V, Majidinia M, *et al.* Differential effects of peroxisome proliferator-activated receptor agonists on doxorubicin-resistant human myelogenous leukemia (K562/DOX) cells. Cell Mol Biol (Noisy-le-Grand). 2015;61(8):118–22.
24. Shafiei-Irannejad V, Samadi N, Salehi R, Yousefi B, Rahimi M, Akbarzadeh A, *et al.* Reversion of multidrug resistance by co-encapsulation of doxorubicin and metformin in poly (lactide-co-glycolide)-d-α-tocopheryl polyethylene glycol 1000 succinate nanoparticles. Pharm Res. 2018;35(6):119.
25. Shojaei S, Ghasemi Z, Shahrisa A. Cu (I)@ Fe3O4 nanoparticles supported on imidazolium-based ionic liquid-grafted cellulose: green and efficient nanocatalyst for multicomponent synthesis of N-sulfonylamidines and N-sulfonylacrylamidines. Appl Organomet Chem. 2017;31(11):e3788.
26. Mir M, Yazdani Y, Asadi J, Khoshbin Khoshnazar AA. Survey on the possibility of utilizing gamma H2AX as a biodosimeter in radiation workers. Iran J Med Phys. 2015;12(1):14–21.
27. Yarmohamadi A, Asadi J, Gharaei R, Mir M, Khoshnazar AK. Valproic acid, a histone deacetylase inhibitor, enhances radiosensitivity in breast cancer cell line. J Radiat Cancer Res. 2018;9(2):86.
28. Yang F, Li G, He Y-G, Ren F-X, Wang G-x. Synthesis, characterization, and applied properties of carboxymethyl cellulose and polyacrylamide graft copolymer. Carbohydr Polym. 2009;78(1):95–9.
29. Lim J, Yeap SP, Che HX, Low SC. Characterization of magnetic nanoparticle by dynamic light scattering. Nanoscale Res Lett. 2013;8(1):381.
30. Anbarasu M, Anandan M, Chinnasamy E, Gopinath V, Balamurugan K. Synthesis and characterization of polyethylene glycol (PEG) coated Fe3O4 nanoparticles by chemical co-precipitation method for biomedical applications. Spectrochim Acta A Mol Biomol Spectrosc. 2015;135:536–9.
31. Huang H, Lai W, Cui M, Liang L, Lin Y, Fang Q, *et al.* An evaluation of blood compatibility of silver nanoparticles. Sci Rep. 2016;6:25518.
32. Dobrovolskaia MA, Clogston JD, Neun BW, Hall JB, Patri AK, McNeil SE. Method for analysis of nanoparticle hemolytic properties in vitro. Nano Lett. 2008;8(8):2180–7.
33. Tso C-p, Zhung C-m, Shih Y-h, Tseng Y-M, Wu S-c, Doong R-a. Stability of metal oxide nanoparticles in aqueous solutions. Water Sci Technol. 2010;61(1):127–33.

34. Corbo C, Molinaro R, Parodi A, Toledano Furman NE, Salvatore F, Tasciotti E. The impact of nanoparticle protein corona on cytotoxicity, immunotoxicity and target drug delivery. Nanomedicine. 2016;11(1):81–100.

35. McGowan JV, Chung R, Maulik A, Piotrowska I, Walker JM, Yellon DM. Anthracycline chemotherapy and cardiotoxicity. Cardiovasc Drugs Ther. 2017;31(1):63–75.